NACA

RESEARCH MEMORANDUM

INVESTIGATION OF PERFORMANCE OF TYPICAL INLET

STAGE OF MULTISTAGE AXIAL-FLOW COMPRESSOR

By Jack R. Burtt

Lewis Flight Propulsion Laboratory
Cleveland, Ohio

NATIONAL ADVISORY COMMITTEE
FOR AERONAUTICS
WASHINGTON
July 18, 1949

NATIONAL ADVISORY COMMITTEE FOR AERONAUTICS

RESEARCH MEMORANDUM

INVESTIGATION OF PERFORMANCE OF TYPICAL INLET

STAGE OF MULTISTAGE AXIAL-FLOW COMPRESSOR

By Jack R. Burtt

SUMMARY

Analysis of basic design variables on the performance of an axial-flow compressor has indicated that the use of a design incorporating constant total enthalpy with symmetrical velocity diagram at all radii has several advantages over the more common vortex-flow-type compressor. An investigation of a typical inlet stage of a multistage axial-flow compressor that was designed on this basis was therefore conducted. The stage, consisting of 19 rotor blades and 20 stator blades with 40 inlet guide vanes, had a hub-to-tip-radius ratio at the rotor inlet of 0.50 and a rotor-blade outside diameter of 14 inches. The ratio of the axial velocity component to the tip speed was set at 0.60 at the rotor-inlet hub. The rotor and stator blades were of constant cross section from hub to tip and had a modified NACA 65-(12)10 profile.

Rotor-blade performance is presented as plots of angle of attack against turning angle and radial distribution of energy addition. The turning angles and, consequently, the energy addition were low compared with design values at design weight flow. This deviation was attributed largely to the fact that too little allowance was made for the decrease in turning angle due to the low solidities and high stagger angles encountered near the rotor-blade tip.

A maximum efficiency of 0.97 at the design speed of 18,060 rpm with a pressure ratio of 1.18 and an air weight flow of 24.5 pounds per second was obtained for the compressor stage. A maximum pressure ratio of 1.28 was reached with an efficiency of 0.90 at design speed with an air weight flow of 21.0 pounds per second. These combinations of weight flow and pressure ratio were good for a compressor stage with a hub-to-tip-radius ratio of 0.50. In addition, the high rotative speed of this inlet-stage design will permit higher pressure ratios over the later stages of a multistage compressor.

The data indicated that the use of a variable-camber blade might have minimized the radial variations in energy addition and permitted the entire blade to work in a region of low drag over a large range of weight flow.

INTRODUCTION

The free-vortex compressor design has been extensively used
because of the simplicity and the accuracy with which the flow can
be calculated. An analysis of the effect of basic design variables
on the performance of axial-flow compressors (reference 1) indicated
that the use of constant total enthalpy with a symmetrical velocity
diagram at all radii has several advantages, the most important of
which are higher pressure ratio per stage and higher mass flow for
a given blade-loading and Mach number limitation. The symmetrical
diagram also results in a smaller radial variation of relative Mach
number across the flow passage at the rotor inlet than that for a
free-vortex design. Thus the limitations of blade loading or turning
and Mach number become less restraining.

In order to study the performance of a compressor stage using
a symmetrical velocity diagram at all radii, the NACA Lewis labo-
ratory designed, built, and investigated a single-stage compressor
that was representative of an inlet stage of a multistage compressor.
A typical inlet stage was chosen for this investigation because the
long blades of an inlet stage enable a greater variation of flow
conditions across the passage and because of the importance of this
stage to the multistage compressor. In general, the quantity and
the type of flow distribution through the inlet stage govern the
flow through a multistage compressor, and the Mach number limitations
set the rotative speed.

The compressor investigated had a 14-inch diameter and a hub-
to-tip-radius ratio of 0.50 at the rotor inlet. The stage consisted
of 19 rotor blades and 20 stator blades with 40 inlet guide vanes
to provide the required prerotation. The rotor and stator blades
were of constant section from hub to tip and used a modified
NACA 65-(12)10 blade profile. The guide vanes were of sheet metal
with a circular-arc camber.

The performance of the compressor was investigated at equiv-
alent speeds of 9030, 13,545, and 18,060 rpm representing one-half
design speed, three-fourths design speed, and design speed, respec-
tively. In addition to the inlet and outlet measurements required
for evaluating the over-all compressor performance, flow measure-
ments were made between blade rows. The stage performance is pre-
sented in curves of adiabatic temperature-rise efficiency and total-
pressure ratio against corrected weight flow for the three speeds.
Rotor-blade-row performance is discussed in terms of radial dis-
tribution of energy addition and the variation of turning angle
with angle of attack.

SYMBOLS

The following symbols are used in the equations and on the figures:

C_L lift coefficient

K constant in turning-angle relation

$N/\sqrt{\theta}$ rotor speed corrected to standard sea-level temperature, (rpm)

P total pressure, (lb/sq ft absolute)

p static pressure, (lb/sq ft absolute)

r radius to blade element, (ft)

U velocity of blade at radius r, (ft/sec)

V absolute air velocity, (ft/sec)

V' air velocity relative to rotor, (ft/sec)

ΔV_θ change in tangential velocity, (ft/sec)

$\dfrac{W\sqrt{\theta}}{\delta}$ weight flow corrected to standard sea-level pressure and temperature, (lb/sec)

w_m ratio of mean whirl velocity to axial velocity

α angle of attack, (deg)

$\alpha_{i,0}$ angle of attack of isolated airfoil for zero lift, (deg)

β absolute stagger angle, angle between compressor axis and absolute air velocity, (deg)

β' relative stagger angle, angle between compressor axis and air velocity relative to rotor, (deg)

$\Delta\beta'$ relative turning angle in rotor, (deg)

δ ratio of inlet total pressure to standard sea-level pressure

θ ratio of inlet total temperature to standard sea-level temperature

ρ density (slugs/cu ft)

σ blade-element solidity, ratio of chord length to distance between adjacent blades

φ blade-angle setting, (deg)

Subscripts:

1   inlet to rotor

2   outlet of rotor

e   referred to equivalent constant axial velocity diagram

m   mean radius

t   tip

z   axial

θ tangential

COMPRESSOR DESIGN

Aerodynamic design. - The aerodynamic design of the compressor is based on constant total enthalpy and a symmetrical velocity diagram at all radii. The design procedure was based on the following initial assumptions:

(1) Density variations within a single stage can be neglected.

(2) Axial velocity is constant at a given radius within a blade row.

(3) Limiting relative Mach number = 0.725 at rotor inlet.

(4) Limiting $\sigma C_L = 0.77$ for rotor.

(5) Ratio $V_z/U_t = 0.6$ at the rotor inlet at the hub.

(6) Radial equilibrium of pressure and centrifugal forces existed at the rotor inlet.

(7) Stage efficiency = 0.89.

Radial equilibrium between the rotor- and stator-blade rows is neglected.

From inlet Mach number and σC_L limitations at the hub, axial and tangential velocity components were calculated for straight-through flow through an untapered passage with a symmetrical diagram. The density ratio over the stage was computed for an assumed vortex-whirl addition in the rotor and an efficiency of 0.89. From continuity, an inner-passage diameter was determined for an axial position corresponding to the inlet of the second-stage rotor. The values of the velocities originally calculated were then corrected by assuming uniform streamline flow through the tapered passage just determined. This correction causes the resultant diagram along a streamline to deviate slightly from the original assumption of a symmetrical diagram. Blade settings, however, were computed with the velocities previously calculated for straight-through flow.

Blade-angle settings were calculated by using the relation between angle of attack and turning angle suggested by Kantrowitz and Daum for a solidity range near unity (reference 2)

$$\Delta\beta' = K \left(\alpha - \alpha_{1,0}\right)$$

where K is a function of solidity and stagger angle and was taken as 0.9 and $\alpha_{1,0}$ equaled -8.28 for the 65-(12)10 blade profile.

When this blade design was formulated, it was accepted that, although the value of $K = 0.9$ is valid near the compressor hub, the decrease in solidity toward the tip would cause the value of K to decrease. The extent to which K decreases for solidities as low as 0.56 and stagger angles above 60° was unknown. The blade settings determined with this equation were therefore arbitrarily reduced $4\frac{1}{2}^\circ$ at the tip and faired to a hub-to-tip-radius ratio of 0.8 to give a higher angle of attack and thus compensate for the decrease in turning due to the reduction in solidity.

Guide vanes for the compressor were 1/16-inch sheet metal and had a circular-arc camber with a constant radius of curvature from hub to tip. The chord was adjusted to give the required turning. Both the rotor and the stator blades used a slight modification of

the NACA 65-(12)10 compressor blade (reference 2). The profile was modified by using a 1-inch radius of curvature in forming the concave part of the lower blade surface near the trailing edge. This modification was a limitation imposed by existing methods of blade fabrication and was of insufficient magnitude to seriously affect the blade-row performance as compared with the true 65-(12)10 blade section. Blade-fabrication tolerances of ±0.002 inch were maintained.

The rotor had a tip diameter of 14 inches and a hub-to-tip-radius ratio of 0.500 at the inlet to the rotor-blade row and 0.567 at the outlet of the stator blades. The axial spacing between blade rows was approximately 0.5 inch. The radial variation of blade data is given in table I.

Mechanical design. - A photograph of the compressor with the top half of the casing removed is shown in figure 1. A part of the bellmouth inlet section containing six streamlined bearing-housing support struts is shown in addition to the guide vanes, the rotor, and the stator blades. The rotor blades were secured in the rotor with a circular dovetail-type joint. Disks on each side of the rotor locked the blades in place axially. The installation of the guide vanes and stator blades in the outer casing is shown in figure 2.

APPARATUS AND PROCEDURE

Compressor Installation

Power was supplied to the compressor shaft by a variable-frequency electric motor capable of supplying 400 horsepower at 20,000 rpm. The speed was maintained constant by an electronic control and was measured with an electronic precision tachometer.

A schematic diagram of the setup is shown in figure 3. Air entered through an orifice tank and a motor-operated inlet throttle into a depression tank 4 feet in diameter equipped with screens to insure a uniform distribution of air at the compressor inlet. Air was discharged from the compressor into a collector that was connected to the altitude-exhaust system by two outlet pipes.

Instrumentation

The instrumentation for this compressor was similar to that described in reference 3. In order to determine the over-all performance of the compressor, inlet flow measurements were made in the inlet depression tank and outlet measurements were made at a station located 0.6 chord length downstream of the stator blades. Because of the size of the inlet depression tank, the pressure and temperature measurements were assumed to be stagnation values. The outlet measurements, including total temperature, total pressure, static pressure, and flow angle were made at four radial points a, b, c, and d located at the centers of four equal spaces across the passage lettered from tip to hub. Four 19-tube circumferential total-pressure rakes each covering a blade passage and each located at one of the radial positions were symmetrically spaced around the compressor.

Four, four-probe shielded thermocouple rakes were equally spaced around the compressor periphery and were differentially connected to the thermocouple in the inlet depression tank to read a circumferentially averaged value of the temperature rise across the stage. Static-pressure and yaw-angle measurements were obtained from radial surveys at a single circumferential position.

Interstage measurements were taken upstream and downstream of the rotor blades at radial stations determined by the same method used for the outlet measurements. These measurements included radial surveys of total pressure, static pressure, and yaw angle at a single circumferential position.

Procedure

The investigation was divided into two phases: (1) with the complete stage and (2) with only the guide vanes and the rotor. The effect of the stator blades on the measuring devices downstream of the rotor necessitated this procedure. Data were taken at constant values of equivalent rotor speed $N/\sqrt{\theta}$ of 9030, 13,545, and 18,060 rpm corresponding to one-half, three-fourths, and design speed. At each speed, a range of air flows was investigated from a flow at which stall occurred to a limiting flow at which a pressure rise was no longer obtained at the tip of the blade. At design speed, this high flow limit could not be obtained because of flow limitations in the exhaust system. An absolute inlet pressure of 25 inches of mercury was used for one-half and three-fourths design speed and an inlet pressure of 23 inches of mercury absolute was used for design speed.

The data presented herein were calculated by the methods presented in reference 4.

Accuracy of Measurements

The estimated accuracy of temperature measurements for these data is $\pm 0.1^{\circ}$ and $\pm 0.5^{\circ}$ F for the inlet and outlet temperatures, respectively. Compressor speed was held constant at each speed within ± 0.15 percent. The absolute air angle at a given radial survey station is accurate within $\pm 0.50^{\circ}$. This accuracy, however, does not include the deviations between the mean value averaged circumferentially and the value obtained at a single circumferential point. These deviations should be small except at extremely high and low angles of attack where separation may occur.

Total pressure is estimated to be accurate within ± 1.0 percent of the dynamic pressure. The velocities determined from static and total pressures have an estimated accuracy of 4 percent. This relatively high error is due both to the effect of adverse flow conditions, such as radial flow and blade wakes, on the static-pressure probe and to the supposition that a survey at one circumferential point is indicative of the average flow about the circumference of the compressor. Calculations have shown that the errors in the velocity components will affect turning angle and angle of attack approximately the same amount and in the same direction. Consequently, these errors cause practically no error in slope or mean values of the curve of turning angle against angle of attack, but affect the limiting points only.

RESULTS AND DISCUSSION

Over-All Compressor Performance

The over-all performance characteristics of the compressor are presented in figure 4. At the design speed of 18,060 rpm, a maximum pressure ratio of 1.281 was obtained at an efficiency of 0.90 and an equivalent weight flow of approximately 21.0 pounds per second. A peak efficiency of 0.97 was reached at a weight flow of 24.5 pounds per second with a total-pressure ratio P_2/P_1 of 1.18.

Inasmuch as the efficiency presented is a weighted average over the main part of the blade and does not include tip-clearance or annulus losses, this efficiency is essentially a mean blade-element efficiency rather than an over-all compressor efficiency. The shape of the efficiency curves and the location of peak points, however, are accurately evaluated by these data.

Inasmuch as no comparable experimental data are available on the relation of pressure ratio and flow capacity in axial-flow

compressor inlet stages, the compressor used in this investigation can be rated only with regard to theoretical considerations. For a given relative Mach number and σC_L limitation, the pressure ratio and flow capacity of an axial-flow compressor stage are functions of the hub-to-tip-radius ratio, the velocity diagram, and the ratio of whirl to axial velocity. In general, a small hub-to-tip-radius-ratio means a large flow area, but for vortex designs the radial variation of relative Mach number and σC_L is large and tends to limit the pressure ratio and flow obtainable. As discussed in reference 1, the use of a symmetrical diagram at all radii results in a more nearly uniform relative Mach number and σC_L from hub to tip and thus gives a good combination of weight flow and pressure ratio. As the ratio of whirl to axial velocity is decreased at a given Mach number and σC_L, the flow capacity is increased but the pressure ratio and the compressor rotative speed are decreased. The decrease in rotative speed in turn decreases the pressure-ratio capacity of the succeeding stages. The ratio of whirl to axial velocity w_m for this design varies from 0.42 at the hub to 1.95 at the blade tip. This range of values represents a compromise that tends to favor high pressure ratio rather than high flow capacity (reference 1) and has a relatively high rotative speed for the given relative Mach number limitation. At the weight flow of 24.5 pounds per second for peak efficiency at design speed, this compressor had an over-all total-pressure ratio of 1.18 and a flow that is 62.4 percent of the maximum flow that would be obtained with sonic axial velocity at the rotor inlet. This combination of weight flow and pressure ratio is excellent for a compressor stage with a hub-to-tip ratio of 0.50.

Comparison of Compressor Performance with Design

Energy addition. - Inasmuch as the design flow at design speed could not be reached, all comparisons of performance with design predictions and all detailed flow studies are made for three-fourths design speed. Analysis of flow over the rotor is based on data without stator blades. The predicted over-all performance at three-fourths design speed is an isenthropic total-pressure ratio of 1.1 at a weight flow of 21.5 pounds per second. From figure 4, the extrapolated experimental pressure ratio obtained for the flow of 21.5 pounds per second is only about 1.02. The principal factors that may cause this discrepancy between design and experimental pressure ratio are: (1) boundary layer at the rotor inlet (2) efficiency of compression, (3) flow distribution at the rotor inlet, and (4) enthalpy addition by the rotor.

The design values of weight flow and pressure ratio are based
on nonviscous ideal-fluid flow. The design conditions at the inlet
of the rotor will therefore occur at a slightly lower flow than the
design value because of the boundary-layer build-up through the
inlet bellmouth and the guide vanes. Measurements indicated that
the displacement thickness of the boundary layer downstream of the
guide vanes is of the order of 0.050 inch at the tip and 0.010 inch
at the hub. This displacement thickness will cause design angle of
attack on the rotor blades to be theoretically obtained at a weight
flow of 21.1 instead of 21.5 pounds per second. At this weight
flow the over-all efficiency (extrapolated) is about 0.70. Appli-
cation of this efficiency to the isentropic pressure ratio gives a
predicted polytropic pressure ratio of 1.07, whereas the experimental
pressure ratio was 1.03 for the corrected design weight flow of
21.1 pounds per second.

For a given rotor design, the pressure ratio obtained will be
a function of the relative Mach number and relative angle of attack
at the rotor inlet. At a given rotor speed, these factors will be
determined by the weight flow, the axial velocity, and the turning-
angle distribution through the inlet guide vanes. The radial vari-
ation of relative Mach number and equivalent angle of attack at the
rotor-blade inlet for a weight flow of 21.1 pounds per second (design
flow) is shown in figure 5. The equivalent angle of attack was based
on an equivalent diagram having a constant axial velocity and, as
recommended in reference 4, utilized the mean of the inlet and outlet
axial velocities and the true tangential components of velocity.
For comparison, the design values of Mach number and angle of
attack for three-fourths design speed are also plotted in figure 5.
Good agreement between the design and actual distributions was
obtained. The inlet Mach number at the blade tip for a weight flow
of 21.1 pounds per second is only slightly higher than design and
at the compressor hub it is slightly lower than design. A compar-
ison of the experimental equivalent angle of attack with design
values indicates that for the weight flow of 21.1 pounds per second,
the experimental angles of attack at the hub were slightly above
design values whereas those at the tip were slightly below. It is
evident that the energy addition anticipated for the given blade
inlet Mach number and angle of attack was not obtained inasmuch as
the discrepancy in angle of attack is small. Figure 6 is a plot of
mean (mass-averaged) total enthalpy addition against corrected
weight flow. This curve shows that the design enthalpy addition
of 90,100 foot-pounds per slug was obtained at a weight flow of
about 19.1 pounds per second instead of 21.1 pounds per second.

Approach to equilibrium. - There are two common methods of
determining the radial distribution of axial velocity at the inlet
to a stator-blade row. One is the assumption that the axial veloc-
ity distribution at the stator inlet is the same as that at the
rotor inlet. This condition is for zero radial flow for an incom-
pressible process. The absolute magnitude of the axial velocities
are then determined from continuity. By this assumption, radial
accelerations are admitted, but the elapsed time for a particle of
air to pass from the rotor inlet to the stator inlet is assumed to
be sufficiently small to render the radial flow negligible. The
second method is to assume that simple-radial equilibrium of static
pressure and centrifugal forces exists. In this case the velocities
at the stator inlet are determined from the simple-radial-
equilibrium equation

$$\frac{1}{\rho} \frac{dp}{dr} = \frac{V_\theta^2}{r}$$

in conjunction with continuity and the energy equation. Radial
accelerations within the blade row are assumed to be sufficiently
large to establish the static pressure for simple equilibrium at
the stator inlet. The complexity of the complete Euler equation
for radial equilibrium makes it expedient to use one of these two
assumptions to obtain a simplified design theory. The actual flow
distribution immediately behind the rotor will, however, probably
fall somewhere between that assuming no change in axial velocity
through the rotor row and that for simple equilibrium. Simple
equilibrium will be more closely approached as the distance
downstream of the rotor is increased.

As was shown in the section Compressor Design, this com-
pressor was designed using the assumption of constant axial veloc-
ity within the blade row.

In order to determine to what extent the actual flow followed
the design assumption of constant axial velocity over the blade
row, curves are plotted in figure 7 comparing the measured axial-
velocity distribution (in terms of velocity ratio $V_z/V_{z,m}$) enter-
ing the rotor at three-fourths design speed and a flow of 18.2 pounds
per second with that obtained at the measuring station downstream
of the rotor. The axial-velocity distribution that would be
expected at the rotor outlet if the flow were in simple-radial equi-
librium using the measured tangential velocities is also plotted.
It is apparent that some radial shift in the flow occurred so as to
change the axial-velocity distribution over the blade row. This

radial flow was not, however, sufficient to satisfy completely the
requirement of simple-radial equilibrium. As was expected, the
actual flow through the rotor lay somewhere between the assumption
of no change in axial-velocity distribution over the rotor row and
the assumption of the existence of simple-radial equilibrium at the
rotor outlet.

Rotor-Row Performance

Radial distribution of energy addition. - A good method to
minimize mixing losses downstream of a compressor rotor and to
facilitate staging is to keep the total enthalpy from hub to tip
constant. This compressor was therefore designed for a vortex
addition by the rotor with constant enthalpy addition across the
passage. Figure 8 is a plot of the rotor enthalpy addition
$\dfrac{U \, \Delta V_\theta}{\theta}$ against radius ratio at the rotor outlet r/r_t for the
range of weight flows covered at three-fourths design speed. At
the high weight flows, the enthalpy addition at the blade tip is
extremely low and increases towards the hub. As the weight flow is
decreased, the enthalpy addition at the tip increases rapidly as
compared with that at the hub. At weight flows of approximately
19 pounds per second, the energy addition is relatively uniform
across the annulus. The weight flows that have the most uniform
energy distribution are in the high-efficiency range. At the low
weight flows, the enthalpy addition continuously decreases from
the tip to the hub. Several interacting factors determine the
shape of the curves in figure 8. Briefly, the more predominate
factors are:

1. The high stagger angles and low solidities at the blade
tip result in a somewhat lower value of the slope of the curve of
turning angle against angle of attack for the tip section than for
the hub section. This effect is offset by the fact that, in gen-
eral, a given change in weight flow causes a much larger change in
angle of attack at the tip than at the hub.

2. The high wheel speed at the rotor tip in conjunction with
the high stagger angles results in a larger change in energy addi-
tion for a given change in turning angle at the tip than at the hub.

3. The effects of radial equilibrium of static pressure on
the flow at the rotor outlet causes a decrease in axial-velocity
ratio at the tip as the flow is decreased, whereas near the hub the

axial-velocity ratio increases with decreasing flow. These velocity changes, when applied to the equivalent diagram, indicate an increase in angle of attack at the tip and a decrease at the hub.

Large variations in energy distribution can apparently result from changes in weight flow with blade designs of this type. It is possible that a poor energy distribution resulting from operation at a point other than design in one stage of a multistage compressor may be reduced in succeeding stages. For optimum performance, however, all stages of a multistage compressor should be carefully matched to avoid mixing losses resulting from operation other than design of one or more stages.

Variation of turning angle with angle of attack. - Comparison of two-dimensional static-cascade and three-dimensional rotor data can be made only for the inner radii of the compressor because of the lack of cascade data for the combination of high stagger angles and low solidities encountered in this design at the outer radii. The comparison of experimental performance with design predictions, however, indicated that the turning angles obtained were considerably below those anticipated. In figure 9, the equivalent turning angle $\Delta\beta_e'$ is plotted against equivalent angle of attack for four radial positions; for comparison, the design values obtained from the equation

$$\Delta\beta' = K (\alpha + 8.28)$$

and including the arbitrary correction for solidity and stagger are shown. The turning angles obtained at all radii were from 4° to 9° below those predicted for straight-through flow. At the outer radii where the solidity is extremely low (0.566 at the tip) and the stagger angles are high, the arbitrary correction for solidity was insufficient. In the region of the hub, the validity of the value of K and of $\alpha_{1,0}$ used to determine the blade-angle setting has been verified by two-dimensional cascade data (reference 4). The discrepancy near the hub (station d) can, however, be partly explained by the radial flows due to the large hub taper. If a developed section of the blade is taken along an approximate streamline obtained by taking equal flow increments at the inlet and outlet of the blade row, the angle between the blade trailing edge and the blade chord will be reduced approximately 5° as a result of the decrease in effective camber due to hub taper and blade twist. At the intermediate stations, the underturning may result from the combined effects of insufficient allowance for decreased solidity, increased stagger, radial flows resulting from hub taper, and unknown induced velocity effects. For large hub tapers, the blade sections

should therefore be layed out along a developed conical surface
that approximates the streamlines rather than along a developed
cylindrical surface, as was done in this design. In addition, a
much greater allowance must be made for the effect of solidity and
stagger on turning than was made in this design.

In figure 9, an arrow indicates the equivalent angle of attack
for the weight flow giving peak efficiency. The high efficiency
obtained at this condition indicates that all sections of the blade
are operating in a relatively low drag region of the angle-of-
attack range. A study of drag and pressure-distribution character-
istics of cascades of blades has shown that for a range of angles
of attack on either side of that for optimum pressure distribution,
efficient blade performance can be obtained. Beyond this range of
angle of attack, the blade drag increases rapidly. For a given
blade section, the angle of attack and resulting turning angle for
optimum performance decreases with decreasing solidity and increasing
stagger. Thus, the wide range of turning angles from hub to tip on
this compressor can be efficiently obtained with a constant-camber
blade over a limited range of weight flow. At the blade-tip section,
the slope of the turning-angle curve increases very rapidly as the
weight flow is increased beyond 20 pounds per second, which corre-
sponds to an angle of attack of approximately 3°. A rapid drop in
enthalpy addition accompanied by an increase in losses results as
the weight flow increases. At the hub the blade appears to have a
tendency to stall at an angle of attack of approximately 17°, and
although the turning angle increases with increasing angle of attack
beyond this value, this increase is probably accompanied by drag
increases.

From these performance characteristics of the tip and hub
sections, it appears that in the range of high-efficiency operation
of the compressor the tip section is operating near the low region
of angle of attack of the efficient blade operating range, whereas
the hub is operating near the high region. Thus, a small variation
in weight flow in either direction tends to cause a relatively large
increase in losses. By the use of a lower cambered blade section
at the tip and a higher cambered blade section at the hub, it would
therefore appear possible to flatten the efficiency curve somewhat
and to minimize the poor radial distribution of energy addition at
the extremes of the flow range.

SUMMARY OF RESULTS

The following results were obtained from experimental operation
of a typical inlet stage of an axial-flow compressor designed on the

1131

basis of constant total enthalpy and symmetrical velocity diagram at all radii:

1. At the design speed of 18,060 rpm, a mean blade-element efficiency of 0.97 was obtained at an equivalent weight flow of 24.5 pounds per second and an over-all total-pressure ratio of 1.18. The maximum pressure ratio obtained was 1.28 at a weight flow of 21.0 pounds per second. These combinations of weight flow and pressure ratio were good for a compressor stage with a hub-to-tip-radius ratio of 0.50. In addition, the high rotative speed of this inlet-stage design will permit higher pressure ratios over the later stages of a multistage compressor.

2. The radial distribution of axial velocity at the measuring station immediately downstream of the rotor was somewhere between the design distribution, which assumed no change in axial velocity through the rotor row, and that distribution which would have been obtained had the flow been in simple-radial equilibrium.

3. The enthalpy addition increased more rapidly at the blade tip than at the hub with decreasing weight flow. In the range of peak efficiency, the design conditions of constant enthalpy at all radii were very nearly achieved.

4. The equation suggested by Kantrowitz and Daum (with constant $K = 0.9$) used in setting the blades was invalid in the range of solidities and stagger angles encountered near the tip section of this design. In general, the turning obtained was 4° to 9° below that predicted by assuming straight-through flow. As a result, the design pressure ratio and peak efficiency were obtained at a flow considerably below that for which the compressor was designed.

5. The data indicate that a variable-camber blade would minimize the radial variations in energy addition and would tend to increase the range of high-efficiency operation over that obtained with this constant-camber blade.

Lewis Flight Propulsion Laboratory,
      National Advisory Committee for Aeronautics,
   Cleveland, Ohio.
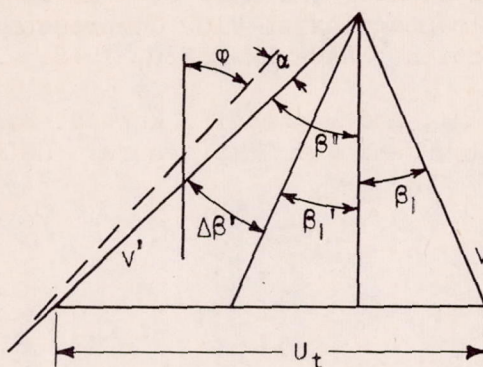
REFERENCES

1. Sinnette, John T., Jr.: Analysis of Effect of Basic Design Variables on Subsonic Axial-Flow-Compressor Performance. NACA Rep. 901, 1948.
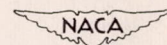
2. Kantrowitz, Arthur, and Daum, Fred L.: Preliminary Experimental
     Investigation of Airfoils in Cascade. NACA CB, July 1942.

3. Mankuta, Harry, and Guentert, Donald C.: Investigation of Per-
     formance of Single-Stage Axial-Flow Compressor Using NACA
     5509-34 Blade Section. NACA RM E8F30, 1948.

4. Bogdonoff, Seymour M., and Bogdonoff, Harriet E.: Blade Design
   Data for Axial-Flow Fans and Compressors. NACA ACR L5F07a,
     1945.

TABLE I - DESIGN DATA OF ROTOR BLADES
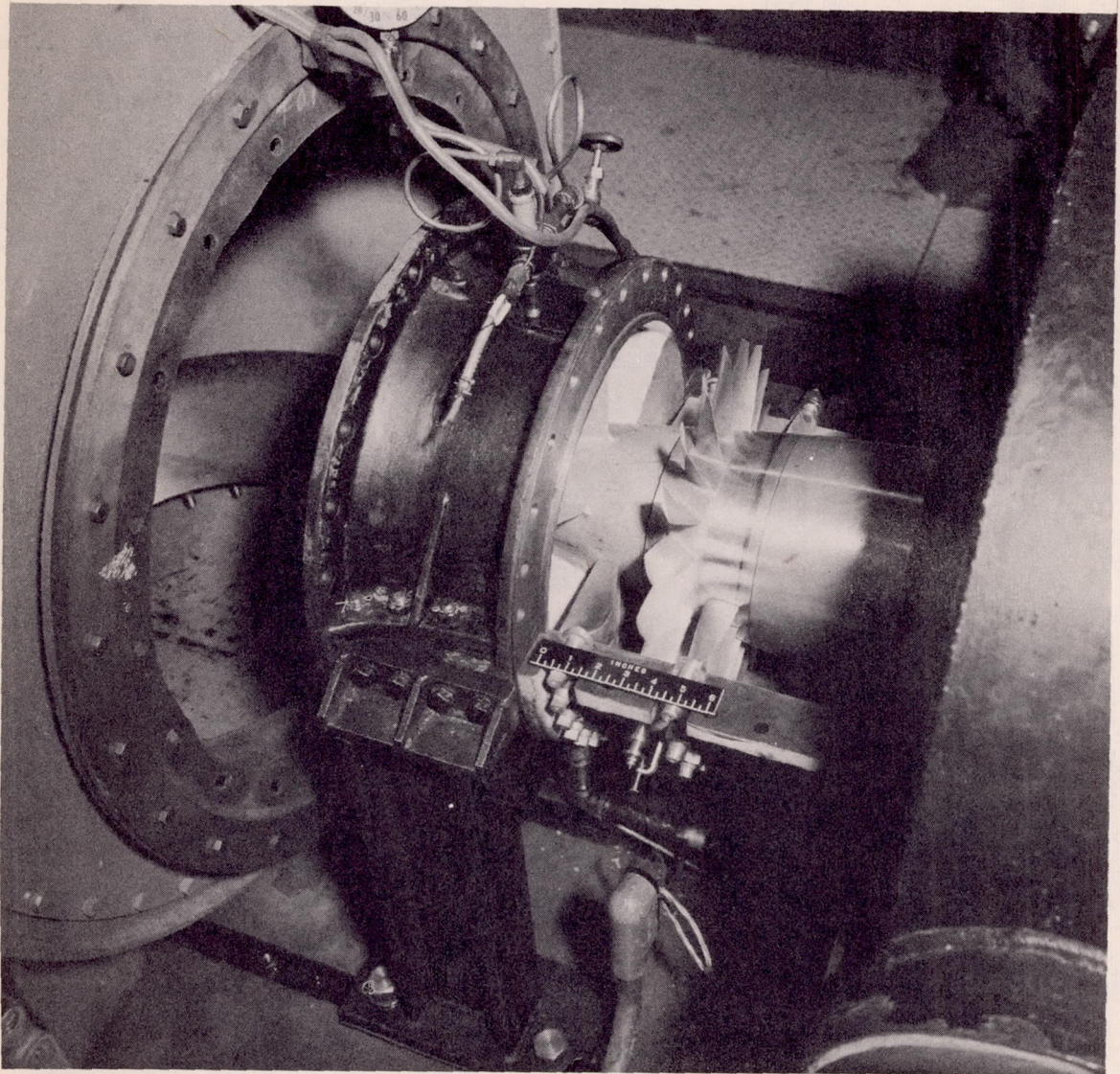
[Chord, 1.310 in.]

Measuring station	Radius ratio At measuring station (1)	Design	Solidity σ	Angle at guide-vane outlet (deg)	Stagger angle β' (deg)	Turning angle $\Delta\beta'$ (deg)	Angle of attack α (deg)	Blade-angle setting φ (deg)
		0.500	1.1318	11.76	32.01	20.25	13.81	18.20
d	0.564		1.0020	16.10	34.00	17.50	11.20	22.30
		.600	.9430	18.86	35.23	16.36	9.73	25.50
c	.689		.8220	25.50	39.00	13.70	6.80	32.15
		.700	.8084	26.14	39.60	13.47	6.50	33.10
		.800	.7074	34.22	45.31	11.09	3.81	41.50
b	.814		.6960	35.80	46.10	10.06	3.40	42.70
		.900	.6288	44.10	52.97	8.82	2.27	50.70
a	.936		.6050	48.50	56.10	7.80	1.90	54.50
		1.000	.5659	58.52	64.54	6.03	1.84	62.70
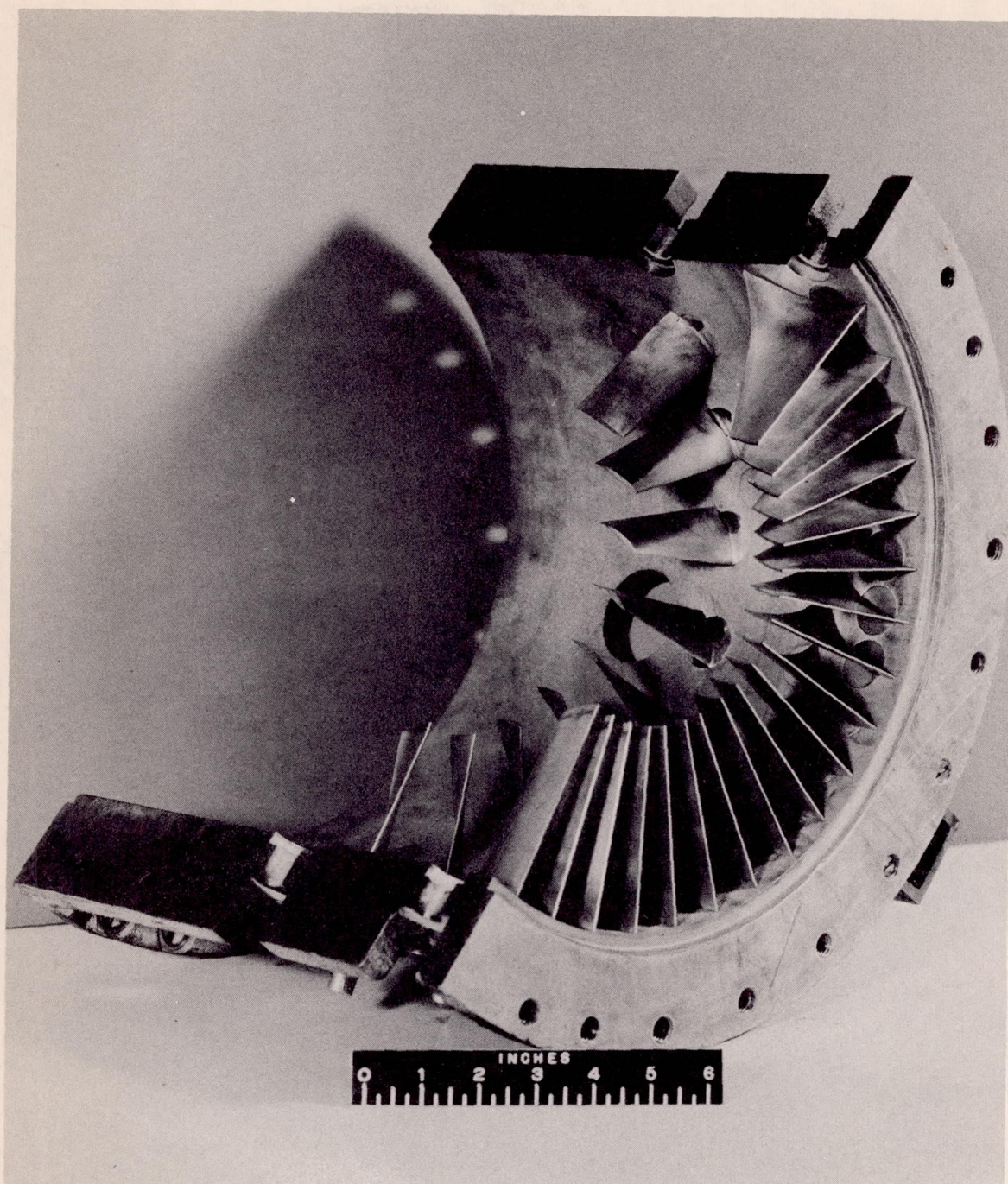
[1]Radius ratio taken at center line of blade on streamline connecting measuring stations upstream and downstream of rotor.

Figure 1. - Compressor with top half of casing removed.

Figure 2. - Guide vanes and stator blades assembled in outer casing.
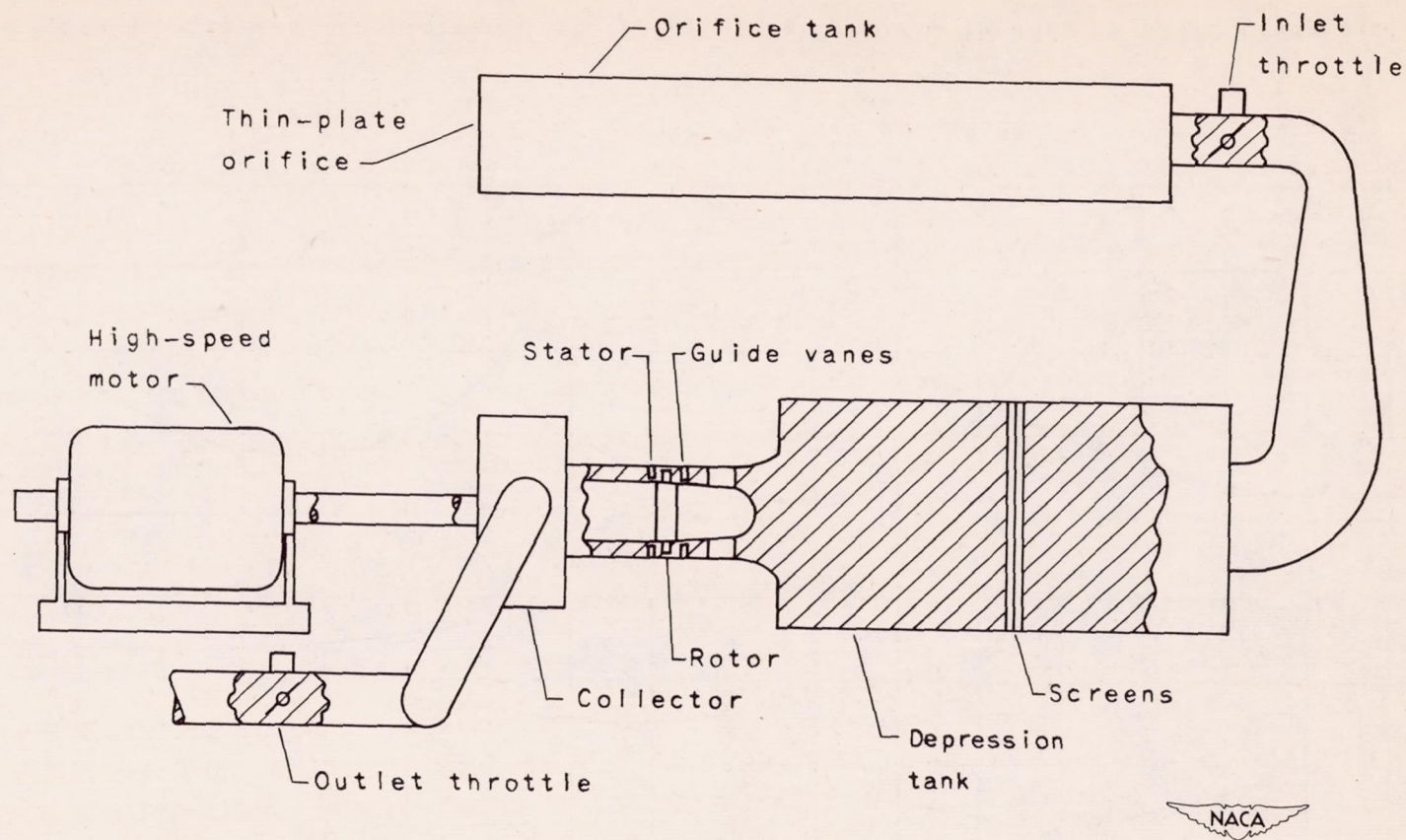
Figure 3. - Schematic diagram of compressor installation.
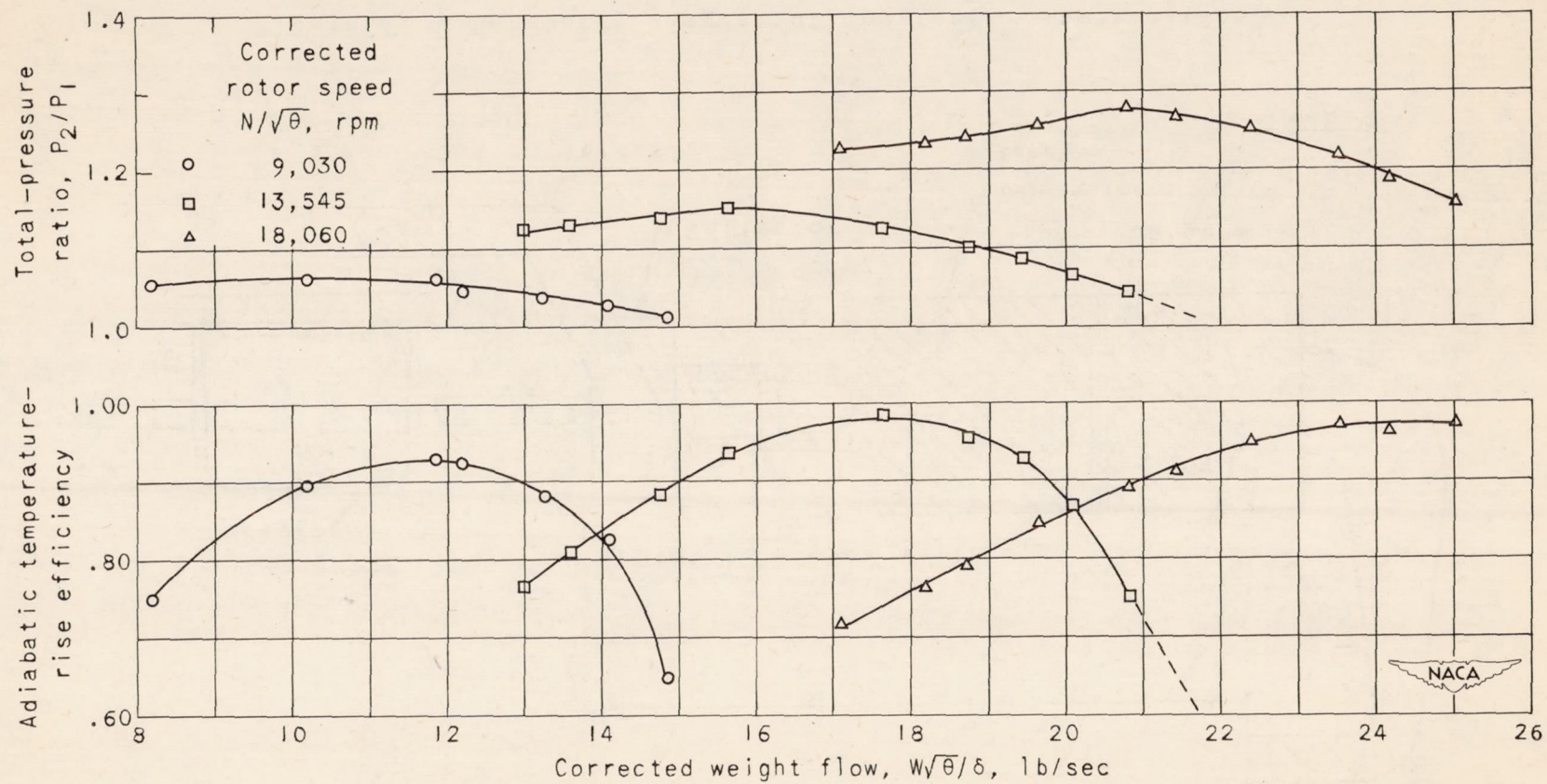
Figure 4. – Over-all performance of typical inlet stage with NACA 65-(2)10 blade section.

1131
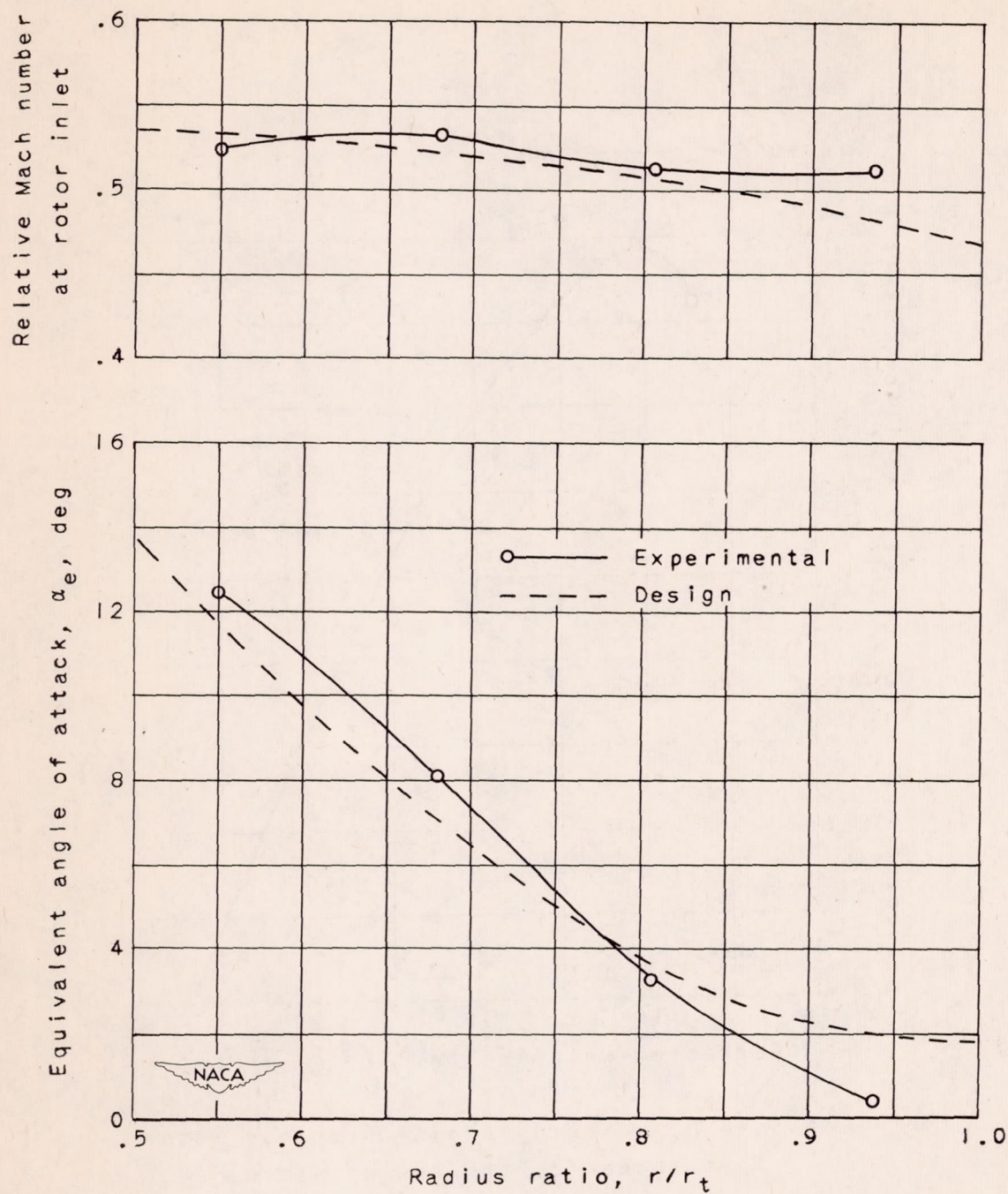
Figure 5. — Angle of attack and Mach number at
corrected weight flow of 21.1 pounds per second
for three-fourths design speed.
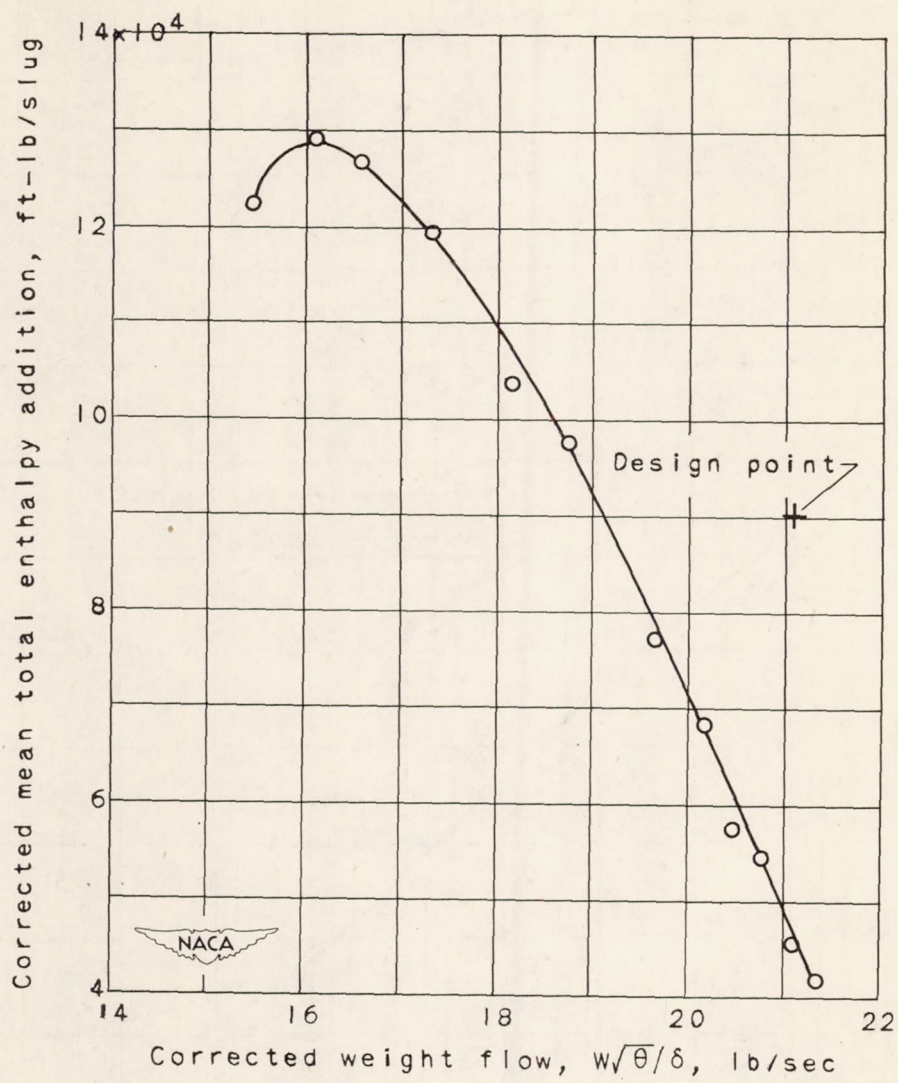
Figure 6. – Energy addition across rotor
at three-fourths design speed.
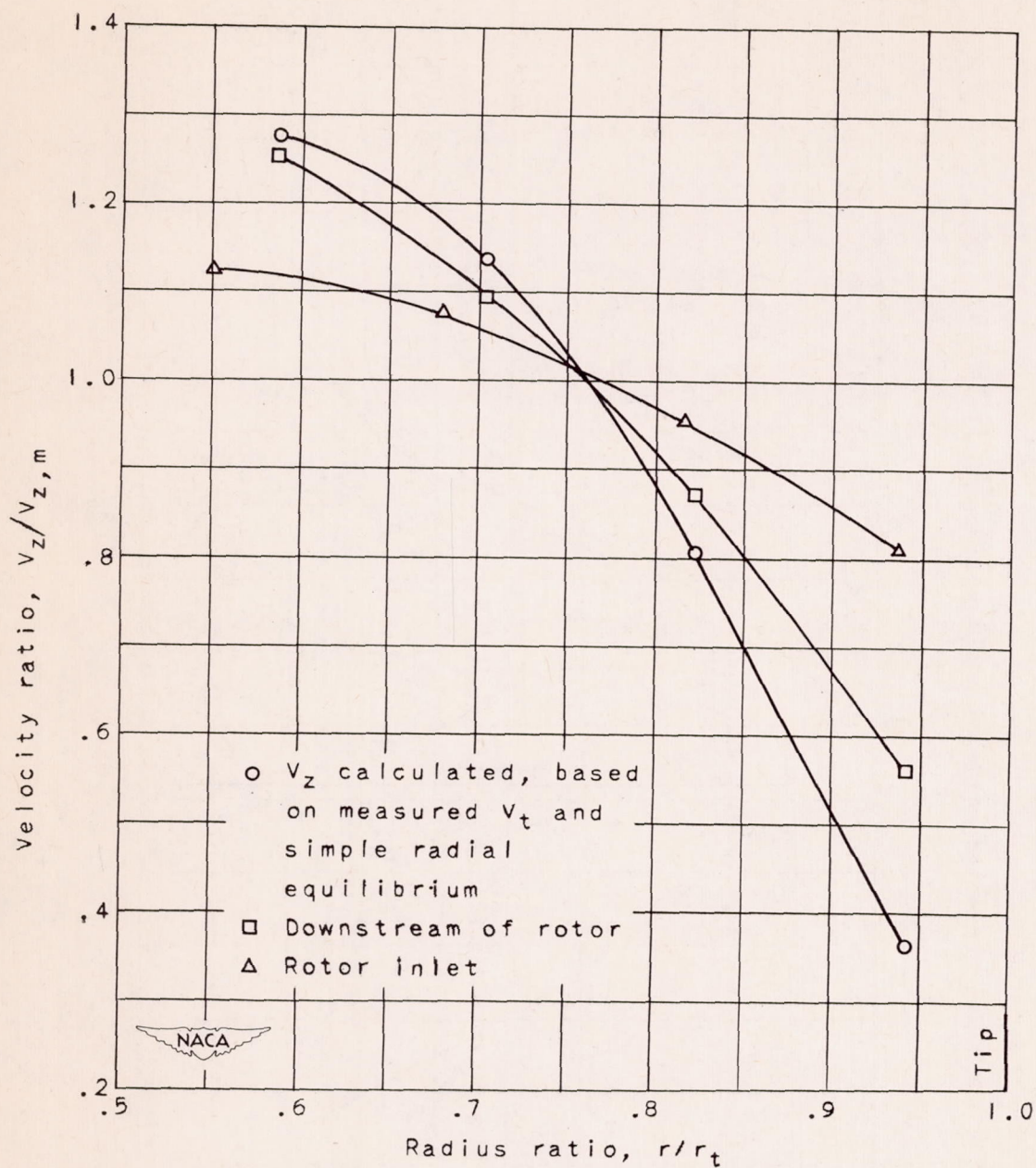
Figure 7. — Axial velocity distribution downstream
of rotor at corrected weight flow of 18.2 pounds
per second for three-fourths design speed.
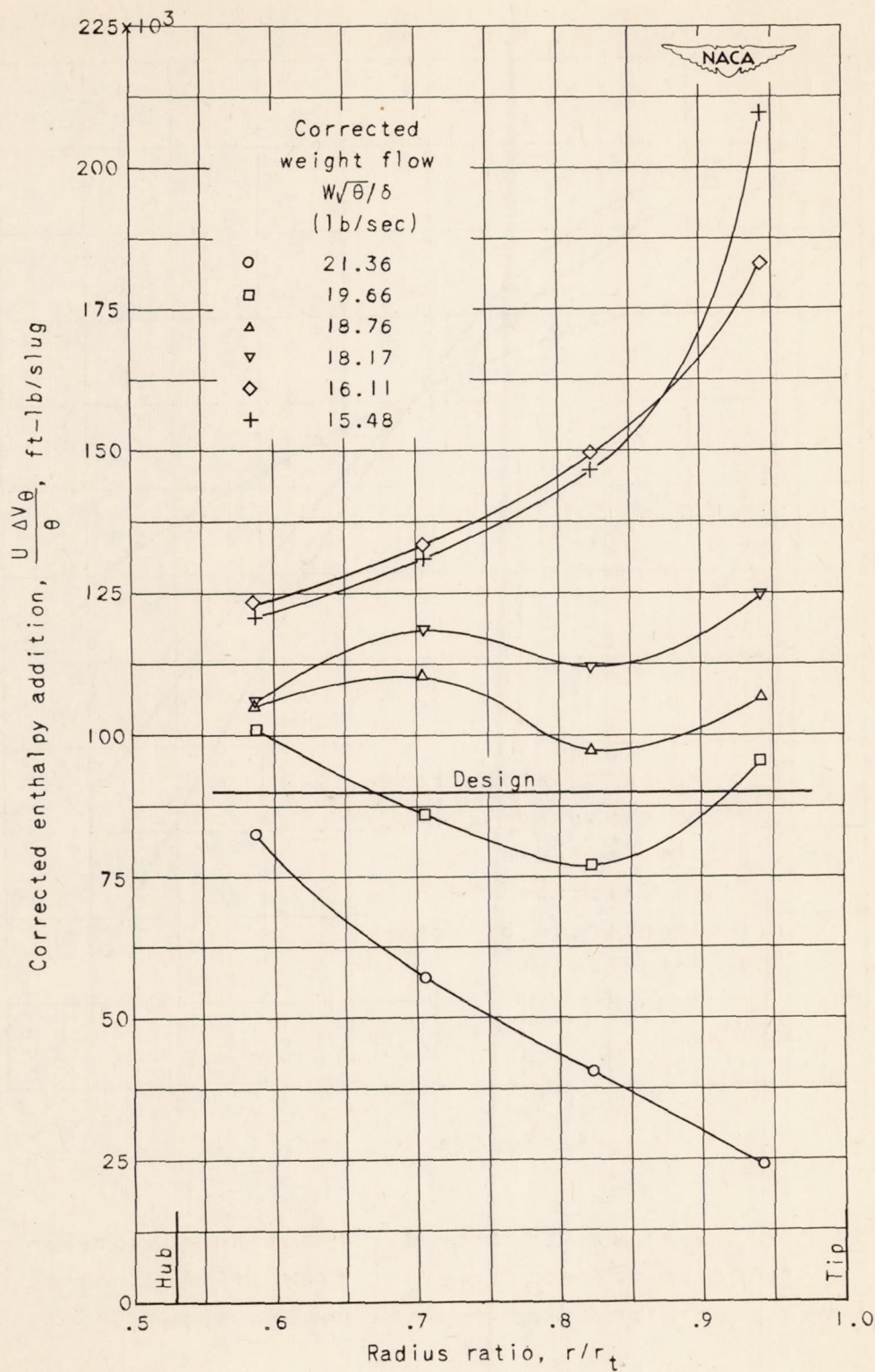
Figure 8. — Radial distribution of energy addition.
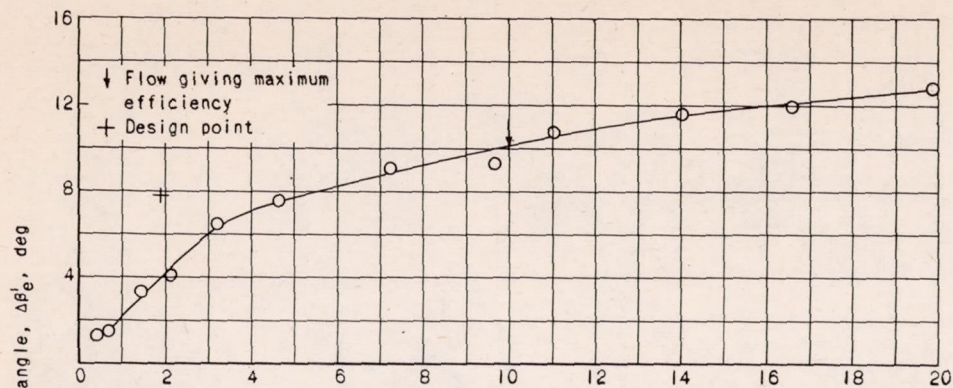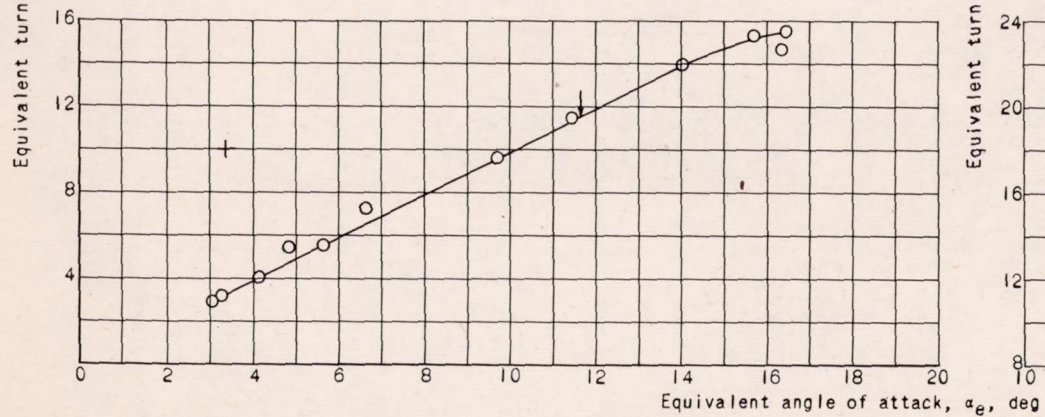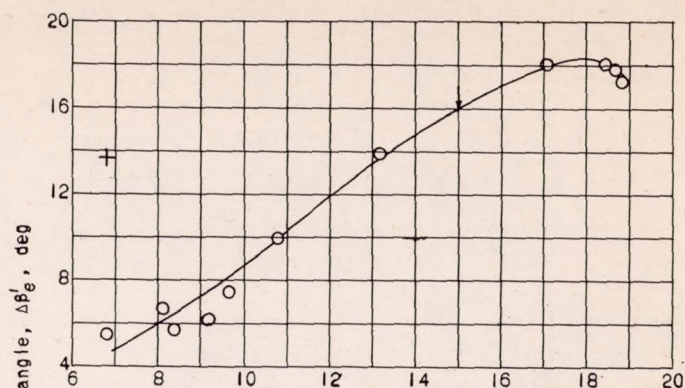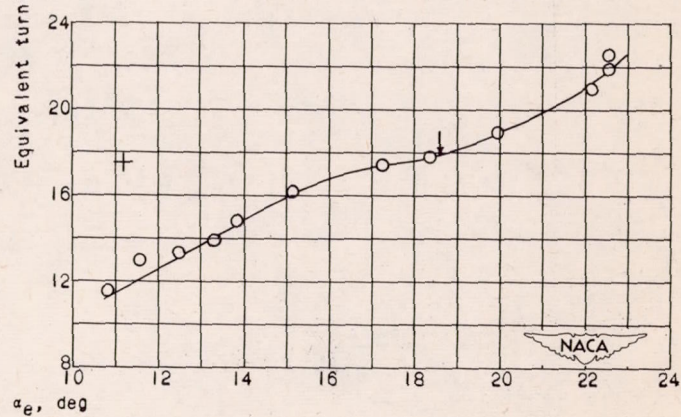
(a) Radial station a near tip, σ = 0.605.

(b) Radial station b , σ = 0.696.

(c) Radial station c , σ = 0.822.

(d) Radial station d near hub, σ = 1.002.

Figure 9. - Equivalent turning angles of rotor blades at three-fourths design speed. NACA 65-(12)10 blade section.